In-situ Decorated Hetero-Composites Derived from Zn(II) based Coordination Polymer Featuring Asymmetric Supercapacitor Application

Arif Ali, Khusboo Kumari, Anupama Joy, Fatma Parween, Mst Shubnur Sultana, Ganesh Chandra Nayak*

Affiliation: *Department of Chemistry & Chemical Biology, Indian Institute of Technology (ISM), Dhanbad, Jharkhand, India-826004*

Corresponding Email: gcnayak@iitism.ac.in

Figure S9	Electrolyte-based comparative study of MZ in 1M KCl, 1M KOH, 1M Na_2SO_4 at 100 mV s^{-1} within potential window range 0.2 to -0.6 V, redox behavior of MZ in aqueous 1M KCl at 2 mVs^{-1} within potential range of 0.2 to -0.6 V
Figure S10	CV profile of (a) GMZ11, GMZ12, GMZ13, and GMZ23, (b) CV profile of RGMZ11, RGMZ12, RGMZ13, and RGMZ23 at 100 mV s^{-1}, (c) Comparative CV profile of best electrode material of GMZ and RGMZ series with MZ at 100 mV s^{-1} within potential window of -0.6 to 0.2 V, (d) plotting of Current density (@ 2, 3, 5, 10, and 20 A g^{-1}) *vs* specific capacitance (F g^{-1})of all prepared electrode materials
Figure S11	Images (a) bare carbon fiber of 3cm × 3cm, (b) coated with active materials, (c) soaked with electrolyte, (d) assembled ASC device
Figure S12	(a) CV and (b) GCD profile of SSC, and ASC device
Figure S13	(a) CV profile of ASC device of MZ, (b) GCD at different current density, (c) EIS spectra of MZ after CV, after GCD and after CS (insert fitted circuit), (d) percentage retention, columbic efficiency (insert CV profile before cyclic stability and after cyclic stability)
Figure S14	(a) CV profile of ASC device of GMZ23, (b) GCD at different current density, (c) EIS spectra of GMZ23 after CV, after GCD and after CS (insert fitted circuit), (d) percentage retention, columbic efficiency (insert CV profile before cyclic stability and after cyclic stability)
Figure S15	FESEM analysis of before and after ASC device at different magnification range, (a,b) before electrochemistry, (c,d) after electrochemistry of MZ; (e,f) before electrochemistry, (g-h) after electrochemistry of GMZ23
Figure S16	EDX analysis of ASC device (a) before and (b) after electrochemistry of GMZ23, (c) before and (d) after electrochemistry of RGMZ11
Figure S17	PXRD pattern after electrochemical performance of MZ, GMZ23, and RGMZ11 (AE: after electrochemistry).

S 1. Material and Methods

S 1.1. Materials

All chemicals were used of analytical grade for analysis as it received. Benzene-1,3-dicarboxylic acid (Isophthalic acid, IPA) and 2-methyl imidazole were procured from TCI India and Sigma Aldrich, respectively. Zinc(II) nitrate hexahydrate ($Zn(NO_3)_2{\cdot}6H_2O$, 99%) was acquired from SRL (Sisco Research Laboratory, India). Graphite flake, median 7-10 microns (99%) was acquired from Alfa Aesar. Dry dimethylsulphoxide (DMSO, 99.5%), Potassium chloride (KCl, 98%) were purchased from SRL, India. Sulfuric acid (H_2SO_4, 37%) was purchased from FINAR, India. Sodium nitrate (Na_2NO_3, 99%) acquired from Merck and hydrogen peroxide (30%) from Avra India, potassium permanganate ($KMnO_4$) from SRL. N-methyl-2-pyrrolidone (NMP) and tetraethylammonium tetrafluoroborate ($TEABF_4$) were

acquired from TCI and Alfa Aesar, respectively. Polyvinylidene fluoride (PVDF, 99.9%) and Carbon Black (CB, 100%) were purchased from Nano Chemazone, Canada, and Alfa Aesar, India, respectively. All chemicals and solvents were utilized without further purification.

S 1.2. Instrumentations

Synthesized materials were characterized by different characterization techniques. Fourier transmittance infra-red (FTIR, PerkinElmer-Spectrum Two), and Raman spectroscopy (LabRAM HR-UV-Open, HORIBA Scientific, France) spectra of MZ and their composites were done. Powder X-ray diffraction (XRD, Rigaku, Smartlab with Cu Kα, Wavelength 1.5406 Å) was utilized to check the bulk phase purity of synthesized materials. Morphological analysis was done utilizing Field Emission Scanning Electron Microscopy (FE-SEM, 55, Carl Zeiss, Germany), and High-Resolution Transmission Electron Microscope (HR-TEM, Thermo Scientific, Talos F200X G2). Energy-dispersive X-ray spectroscopy (EDX)-Mapping (Hitachi, S-3400N). The thermal analyzer "NETZSCH STA 449 F3 Jupiter" instrument was utilized to check the thermal stability of framework composition. X-ray photoemission Spectroscopy (XPS, PHI, 5000 versa probe III) was utilized to analyze the chemical analysis of surface chemistry. All three, two electrode studies were performed on an electrochemical workstation (Metrohm Autolab M204).

S 1.3. Single Crystal X-ray diffraction (SC-XRD)

SC-XRD data of MZ was collected on a 'Supernova, Rigaku Oxford Diffraction' at 100(2) K diffractometer using monochromatic Mo-Kα radiation (λ = 0.71073 Å). The crystal structure of a single crystal was determined using Olex2,[1] solved using olex-2.solve,[2] and refined using olex2.refine.[2] Hydrogen atoms were refined isotropically, while non-H atoms were refined with an anisotropic displacement parameter. Tables S1-S3 summarize the crystal structure refinement data.

S 1.4. Electrochemical Analysis

All electrochemical analyses of all electrode materials for three-electrode and two-electrode studies were performed on an electrochemical workstation (Metrohm Autolab). The electrochemical analysis in a three-electrode system was executed in an aqueous (1 M KOH, and 1 M KCl) electrolyte. Active materials were coated on graphite rod as working electrode, and Ag/AgCl electrode and Pt foil were used as reference and counter electrodes, respectively. To fabricate the working electrode, a slurry of active materials (80 wt%), CB (10 wt%), and PVDF (10 wt%) were mixed with the addition of a few drops of NMP, and drop-casting on the surface of an acid-cleaned graphite rod. Cyclic voltammetry (CV) and the galvanostatic charging–discharging (GCD) study were carried out within a potential range of -0.6 to 0.2 V, to execute the activeness of synthesized materials as anode. The amount of active material was 0.4 mg. The frequency of 1 MHz to 1 Hz at 10 mV amplitude at room temperature was conducted to evaluate the electrochemical impedance spectroscopy (EIS) analysis. The Charging-discharging plot (GCD) was conducted to evaluate the Specific Capacitance (Sp. Cp. in F g^{-1}; C) utilizing eq. [1]:[3]

$$C = (i \times \Delta t)/(m \times \Delta V) \quad (1)$$

The specific capacity Qs (C g^{-1}) was calculated by using the equation (2), since NF exhibits battery type behavior.[4]

$$Qs = (I \times \Delta t)/\, m \quad (2)$$

Where, i = charging-discharging current, Δt = discharge cycle (in second), m = total loaded mass of active material, and ΔV = voltage range.

The specific energy density (ED) (E in Wh kg^{-1}) and power density (PD) (P in W kg^{-1}) were evaluated using the following equations [3,4]:[5]

$$\text{ED, } E = [C(\Delta V)^2]/7.2 \quad (3)$$

$$\text{PD, } P = [E \times 3600]/\Delta t \quad (4)$$

Table S1. Crystal data and structure refinement for MZ.	
CCDC No.	2385212
Empirical formula	$C_{16}H_{16}N_4O_4Zn$
Formula weight	393.73
Temperature/K	293(2)
Crystal system	monoclinic
Space group	$P2_1/c$
a/Å	10.1659(4)
b/Å	10.2917(4)
c/Å	16.6225(6)
α/°	90
β/°	103.761(4)
γ/°	90
Volume/Å^3	1689.20(12)
Z	4
ρ_{calc}g/cm^3	1.5480
μ/mm^{-1}	1.483
F(000)	809.6
Crystal size/mm^3	0.45 × 0.23 × 0.16
Radiation	Mo Kα (λ = 0.71073)
2Θ range for data collection/°	4.12 to 58.92
Index ranges	$-13 \leq h \leq 9$, $-8 \leq k \leq 14$, $-22 \leq l \leq 21$
Reflections collected	8976
Independent reflections	3945 [R_{int} = 0.0218, R_{sigma} = 0.0305]
Data/restraints/parameters	3945/0/229
Goodness-of-fit on F^2	1.041
Final R indexes [I>=2σ (I)]	R_1 = 0.0288, wR_2 = 0.0678
Final R indexes [all data]	R_1 = 0.0361, wR_2 = 0.0712
Largest diff. peak/hole / e Å^{-3}	0.32/-0.54

Table S2. Bond Lengths for MZ.

Atom	Atom	Length/Å		Atom	Atom	Length/Å
Zn1	O1	1.9391(13)		C4	C3	1.343(3)
Zn1	N1	1.9959(15)		C10	C9	1.505(3)
Zn1	N3	2.0048(15)		C10	C15	1.392(3)
Zn1	O3	1.9676(13)		C10	C11	1.390(2)
O1	C9	1.274(3)		C16	C12[1]	1.504(3)
N1	C8	1.386(2)		C6	N2	1.344(2)
N1	C6	1.327(2)		C6	C5	1.481(3)
N3	C4	1.385(2)		N2	C7	1.365(3)

N3	C2	1.326(2)		C9	O2	1.229(2)
O3	C16	1.274(2)		C13	C12	1.391(3)
N4	C2	1.340(2)		C13	C14	1.381(3)
N4	C3	1.365(3)		C12	C11	1.392(2)
O4	C16	1.231(2)		C14	C15	1.384(3)
C8	C7	1.346(3)		C2	C1	1.487(3)

Table S3. Bond Angles for MZ.

Atom	**Atom**	**Atom**	**Angle/°**		**Atom**	**Atom**	**Atom**	**Angle/°**
N1	Zn1	O1	112.97(6)		C12[1]	C16	O3	115.52(16)
N3	Zn1	O1	116.97(6)		C12[1]	C16	O4	120.26(18)
N3	Zn1	N1	110.40(6)		N2	C6	N1	109.43(17)
O3	Zn1	O1	103.48(6)		C5	C6	N1	127.27(17)
O3	Zn1	N1	115.25(6)		C5	C6	N2	123.30(17)
O3	Zn1	N3	96.70(6)		C7	N2	C6	108.77(17)
C9	O1	Zn1	128.81(13)		C10	C9	O1	115.11(17)
C8	N1	Zn1	124.61(13)		O2	C9	O1	125.52(19)
C6	N1	Zn1	128.87(13)		O2	C9	C10	119.3(2)
C6	N1	C8	106.51(16)		N2	C7	C8	106.24(18)
C4	N3	Zn1	121.93(12)		C14	C13	C12	120.02(19)
C2	N3	Zn1	131.69(13)		C13	C12	C16[2]	120.31(17)
C2	N3	C4	106.35(16)		C11	C12	C16[2]	120.11(16)
C16	O3	Zn1	118.82(13)		C11	C12	C13	119.57(18)
C3	N4	C2	108.76(17)		C15	C14	C13	120.21(19)
C7	C8	N1	109.04(18)		C14	C15	C10	120.55(18)
C3	C4	N3	109.14(18)		C12	C11	C10	120.60(17)
C15	C10	C9	120.75(17)		N4	C2	N3	109.54(17)
C11	C10	C9	120.23(17)		C1	C2	N3	126.39(18)
C11	C10	C15	119.00(18)		C1	C2	N4	124.07(18)
O4	C16	O3	124.22(19)		C4	C3	N4	106.21(18)

Table S4. HR-TEM EDX analysis (atomic %) of MZ, GMZ23, and RGMZ11.

Atomic %	**MZ**	**GMZ23**	**RGMZ11**
C	87.4	82.38	87.92
N	5.85	1.24	1.33
O	5.78	6.57	10.46
Zn	0.95	0.16	0.28

Table S5. XPS fitting results with corresponding peak area and percentage of different chemical bonds of MZ, GMZ23, and RGMZ11.

Name	Elemental Atomic %	Assigned Chemical Bond	Area and percentage (%)
MZ	**C1s** = 61.5	C-C/C=C	5321.01 & 37.29%
		C-N	4524.83 & 31.71%
		C-O	1784.28 & 12.50%
		O-C=O	2636.62 & 18.48%
	N1s = 10.0	N-Zn	1164.48 & 29.97%
		N-C	2349.50 & 60.48%
		N-H	370.30 & 9.53%
	O1s = 16.5	C-O	4564.94 & 43.06%
		C=O	3158.24 & 29.79%
		Zn-O	2875.98 & 27.13%
	Zn2p = 12.0	Zn-N ($2p_{3/2}$)	4799.89 & 29.29%
		Zn-O ($2p_{3/2}$)	5576.03 & 34.03%
		Zn-N ($2p_{1/2}$)	2873.25 & 17.53%
		Zn-O ($2p_{1/2}$)	3135.18 & 19.13%
GMZ23	**C1s** = 67.1	C-C/C=C	3088.28 & 16.89%
		C-N	3529.88 & 19.30%
		C-O	4130.46 & 22.59%
		O-C=O	7533.16 & 41.20%
	N1s = 8.6	N-Zn	1016.28 & 30.56%
		N-C	929.42 & 27.95%
		N-H	1007.32 & 30.30%
		Graphitic N	371.17 & 11.17%
	O1s = 20.4	C-O	4215.19 & 31.92%
		C=O	2818.20 & 21.34%
		Zn-O	6171.81 & 46.73%
	Zn2p = 3.9	Zn-N ($2p_{3/2}$)	1641.37 & 29.99%
		Zn-O ($2p_{3/2}$)	1869.65 & 34.17%
		Zn-N ($2p_{1/2}$)	1354.42 & 24.75%
		Zn-O ($2p_{1/2}$)	606.07 & 11.07%
RGMZ11	**C1s** = 69.6	C-C/C=C	4918.72 & 24.42%
		C-N	2990.55 & 14.85%
		C-O	4549.90 & 22.59%
		O-C=O	7675.18 & 38.12%
	N1s = 6.6	N-Zn	1169.57 & 39.07%
		N-C	430.11 & 14.37%
		N-H	1059.14 & 35.38
		Graphitic N	334.10 & 11.16%
	O1s = 18.1	C-O	2746.91 & 22.62%
		C=O	4899.83 & 40.35%
		Zn-O	4495.33 & 37.02%
	Zn2p = 5.7	Zn-N ($2p_{3/2}$)	3668.01 & 33.86%
		Zn-O ($2p_{3/2}$)	3153.66 & 29.11%

		Zn-N ($2p_{1/2}$)	1342.73 & 12.39%
		Zn-O ($2p_{1/2}$)	2666.99 & 24.62%

Table S6: Comparative GCD (Specific capacitance (F g^{-1}), Energy density (Wh kg^{-1}), Power Density (W kg^{-1}), analysis of MZ and GMZ23 ASC devices.

S. No.	Current Density (A g^{-1})	MZ				GMZ23			
		Sp. Cp. (F g^{-1})	Sp. Cp. (C g^{-1})	E.D. (Wh kg^{-1})	P.D. (W kg^{-1})	Sp. Cp. (F g^{-1})	Sp. Cp. (C g^{-1})	E.D. (Wh kg^{-1})	P.D. (W kg^{-1})
1	0.2	13.79	22.06	4.90	160	143.51	229.61	51.02	160
2	0.3	12.62	20.19	4.48	240	129.96	207.93	46.21	240
3	0.4	12.01	19.21	4.27	320	119.86	191.77	42.61	320
4	0.5	11.64	18.62	4.13	400	114.34	182.94	40.65	400
5	1.0	10.18	16.28	3.62	800	85.78	137.248	30.50	800
6	2.0	8.56	13.69	3.04	1600	57.25	91.61	20.35	1600

Table S7: Fitted data value of Nyquist impedance of MZ and GMZ23 ASC devices.

Elements	MZ			RGMZ23		
	After CV	After GCD	After CS	After CV	After GCD	After CS
R_s (Ω)	13.9	11.9	9.9	16.6	24	16.5
R_{CT} (Ω)	-	-	-	3.03	9.22	-
CPE (mMho.S^N)	2.2	1.6	1.7	108	188	173
C_{dl}(μF)	39.8	42.9	38.8	6.29	6.57	
W (mMho.$S^{1/2}$)	253	303	300	181	238	90.7
N	0.52	0.35	0.53	0.67	0.82	0.02

Table S8. Comparison of Electrochemical properties with reported results.

MOF based devices	Electrolyte	Potential window **(V)**	Sp. Cp. **(F g^{-1})**	Current density **(A g^{-1})**	E. D. **(Wh kg^{-1})**	P.D. **(W kg^{-1})**	Retention of Sp. Cp. **(%)**	No. of cycles	Ref.
MOFZP	3 M	1.8	130	1.0	58.4	450	-	10000	6

@rGO2	H_2SO_4								
MOF5-GO (3E)	6 M KOH	0.8	108.45	3.0	-	-	86.5	2000	7
ZMG-1	3 M KOH	0.75	58.3	1.0	4.55	104.17	99.87	2000	8
$NCG_{0.5}$	3 M KOH	1.6	66.8	0.5	23.76	399.95	92.0	1000	9
rGO/Ppy/Zn-MOF	6 M KOH	1.0	175	1.0	19.7	1792	81	7000	10
Ni-MOF@GO	6 M KOH	0.4	111.4	2.0	30.7	388.5	84	7000	11
Ni-MOF/G	6 M KOH	1.5	126.2	2.0	39.43	34.29	73.6	1000	12
ZIF-67/rGO	1 M Na_2SO_4 + 0.2 M K3[Fe(CN)6	0.6	326	3.0	25.5	2.7	88	1000	13
Zn–CP/rGO	2 M KOH	1.55	192	1.0	13.3	789	86	10000	14
Zn-MOF-rGO20	3 M KOH	0.8	82.5	0.5	7.1	400	87	5000	15
RGMZ11	1 M $TEABF_4$ /DMSO	1.6	154.53 (247.48 C g^{-1})	0.2	54.99	160	75	10000	This work

References

1 O. V. Dolomanov, L. J. Bourhis, R. J. Gildea, J. A. K. Howard and H. Puschmann, *J. Appl. Crystallogr.*, 2009, **42**, 339–341.

2 L. J. Bourhis, O. V. Dolomanov, R. J. Gildea, J. A. K. Howard and H. Puschmann, *Acta Crystallogr. Sect. A Found. Adv.*, 2015, **71**, 59–75.

3 Basree, A. Ali, G. C. Nayak, K. A. Siddiqui and M. Ahmad, *ACS Omega*, , DOI:10.1021/acsomega.4c08913.

4 M. Sethi, U. S. Shenoy and D. K. Bhat, *Nanoscale Adv.*, 2020, **2**, 4229–4241.

5 S. De, C. K. Maity, S. Sahoo and G. C. Nayak, *ACS Appl. Energy Mater.*, 2021, **4**, 3712–3723.

6 V. K. Ravi, P. Vickraman and T. A. Raja, *Phys. status solidi*, , DOI:10.1002/pssa.202300210.

7 M. Yadav, I. Saini, S. Sharma, P. Chand, N. Shekhawat and A. Joshi, *Ionics (Kiel).*, , DOI:10.1007/s11581-024-05849-y.

8 S. Tan, Z. Yao, Z. Liu, L. Li and H. Huang, *Ionics (Kiel).*, 2024, **30**, 1051–1060.

9 H. Zhang, L. Yang, X. Li, Y. Ping, J. Han, S. Chen and C. He, *Dalt. Trans.*, 2024, **53**, 4680–4688.

10 N. Saxena, M. P. Bondarde, K. D. Lokhande, M. A. Bhakare, P. S. Dhumal and S. Some, *Chem. Phys. Lett.*, 2024, **856**, 141605.

11 R. Sahoo, S. Ghosh, S. Chand, S. Chand Pal, T. Kuila and M. C. Das, *Compos. Part B Eng.*, 2022, **245**, 110174.

12 M. Azadfalah, A. Sedghi and H. Hosseini, *J. Mater. Sci. Mater. Electron.*, 2019, **30**, 12351–12363.

13 S. Sundriyal, V. Shrivastav, H. Kaur, S. Mishra and A. Deep, *ACS Omega*, 2018, **3**, 17348–17358.

14 T. K. Ghosh and G. Ranga Rao, *Dalt. Trans.*, 2023, **52**, 5943–5955.

15 Q. V. Thi, S. A. Patil, P. K. Katkar, I. Rabani, A. S. Patil, J. Ryu, G. Kolekar, N. T. Tung and D. Sohn, *Synth. Met.*, 2022, **290**, 117155.

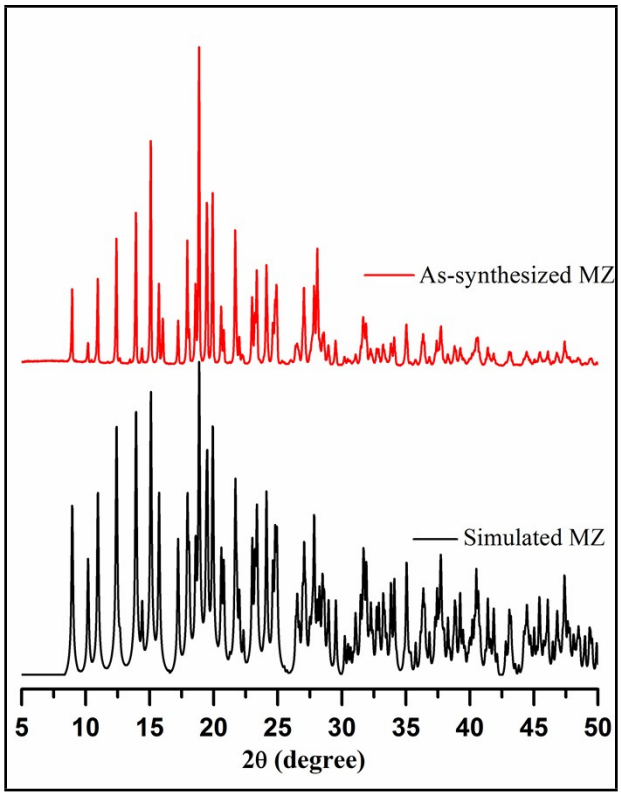

Figure S1. Simulated and as-synthesized pattern of MZ.

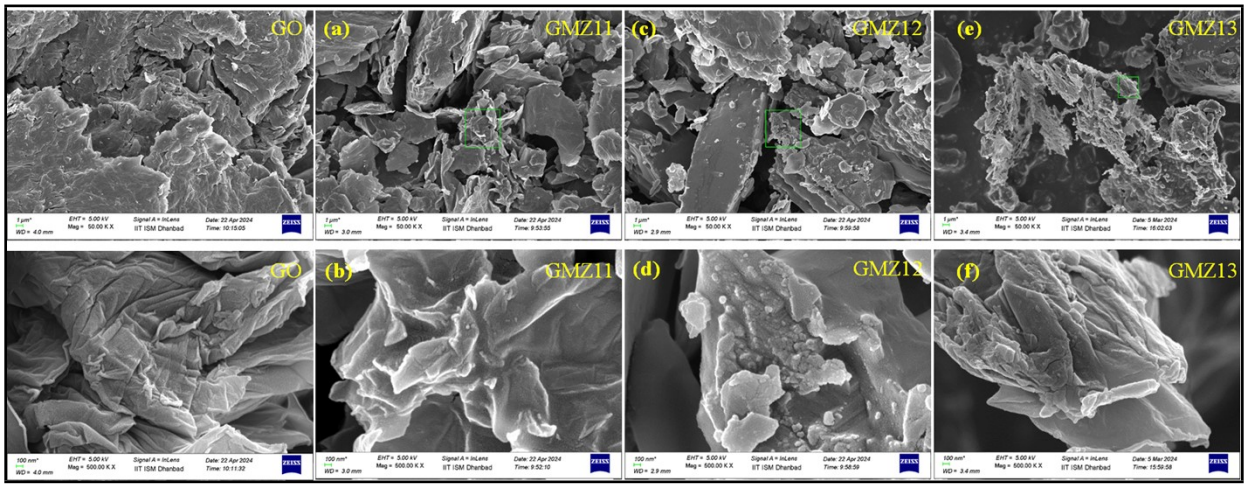

Figure S2. FE-SEM images of GO, GMZ11, GMZ12, and GMZ13 at different magnification range.

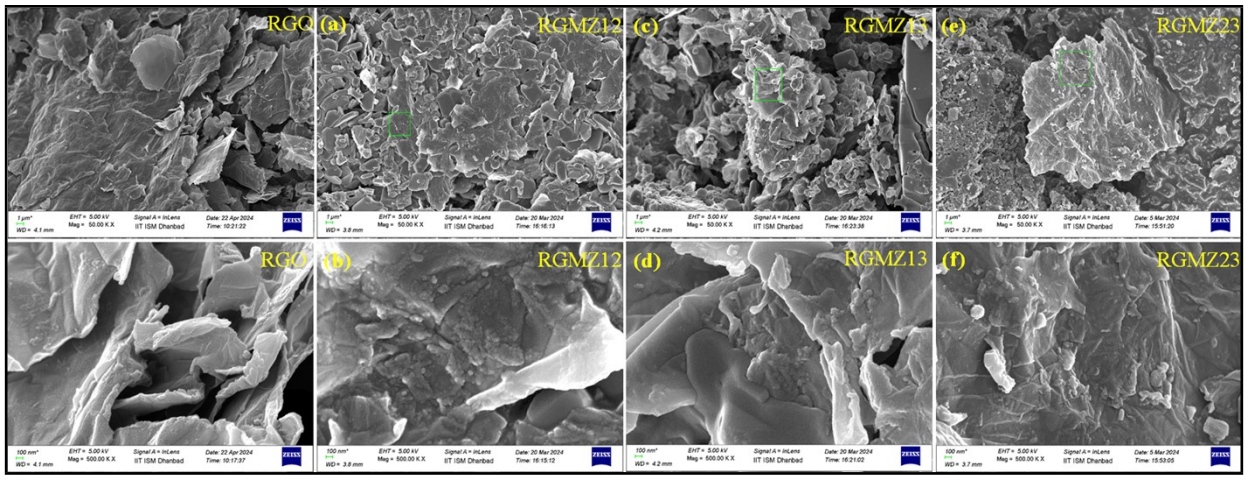

Figure S3. FESEM images of RGO, RGMZ12, RGMZ13, and RGMZ23 at different magnification range.

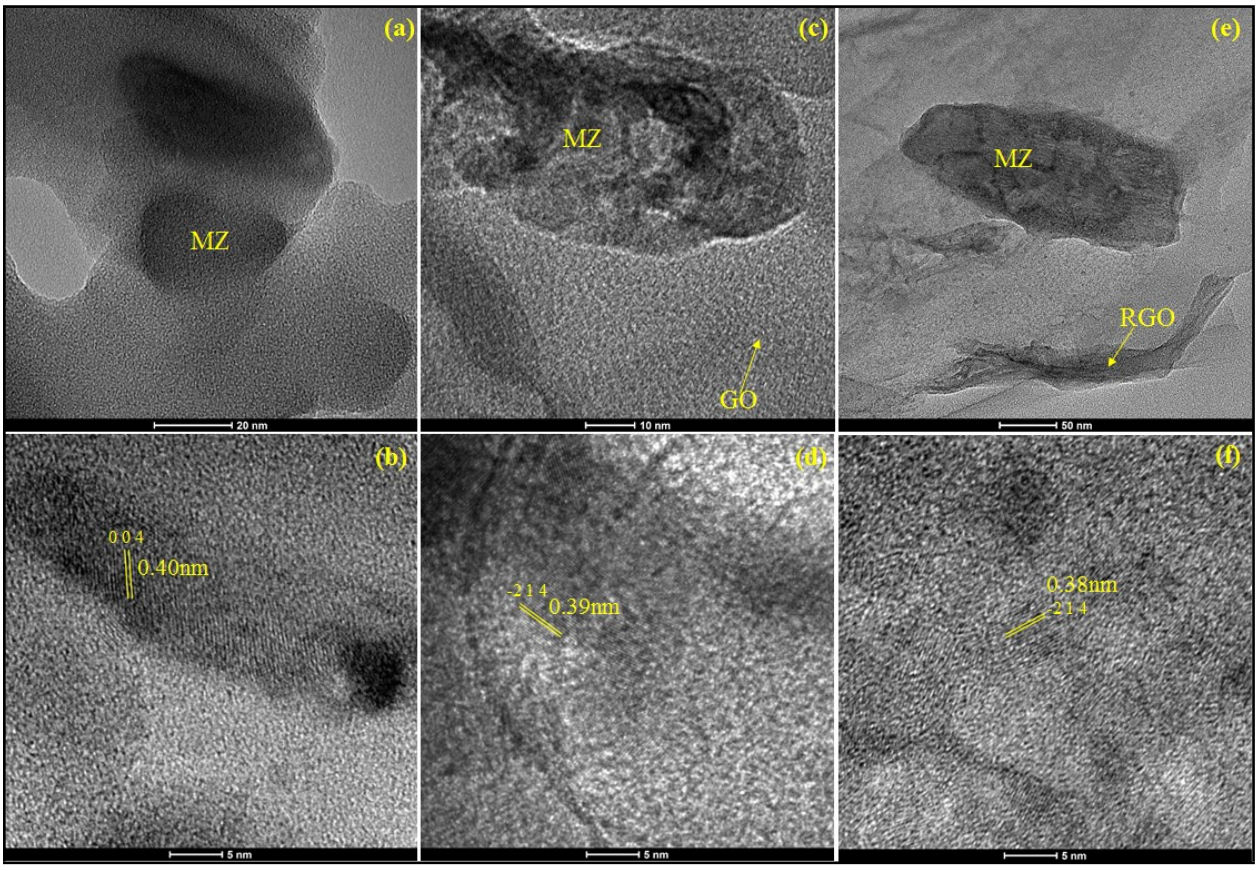

Figure S4. d-spacing value with the targeted area (a,b) MZ, (c,d) GMZ23, and (e,f) RGMZ11.

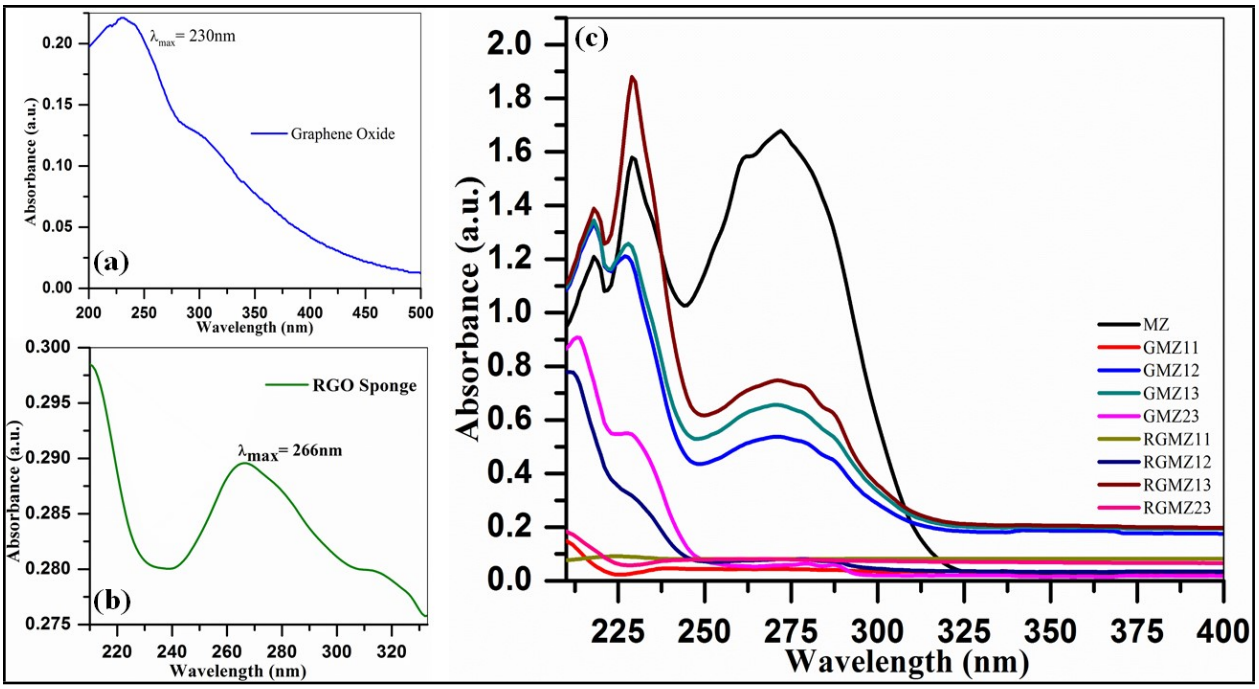

Figure S5. UV-Visible spectra: (a) Graphene oxide; (b) hydrothermally reduced graphene oxide (RGO sponge), (c) combined spectra of MZ and GO, RGO composites.

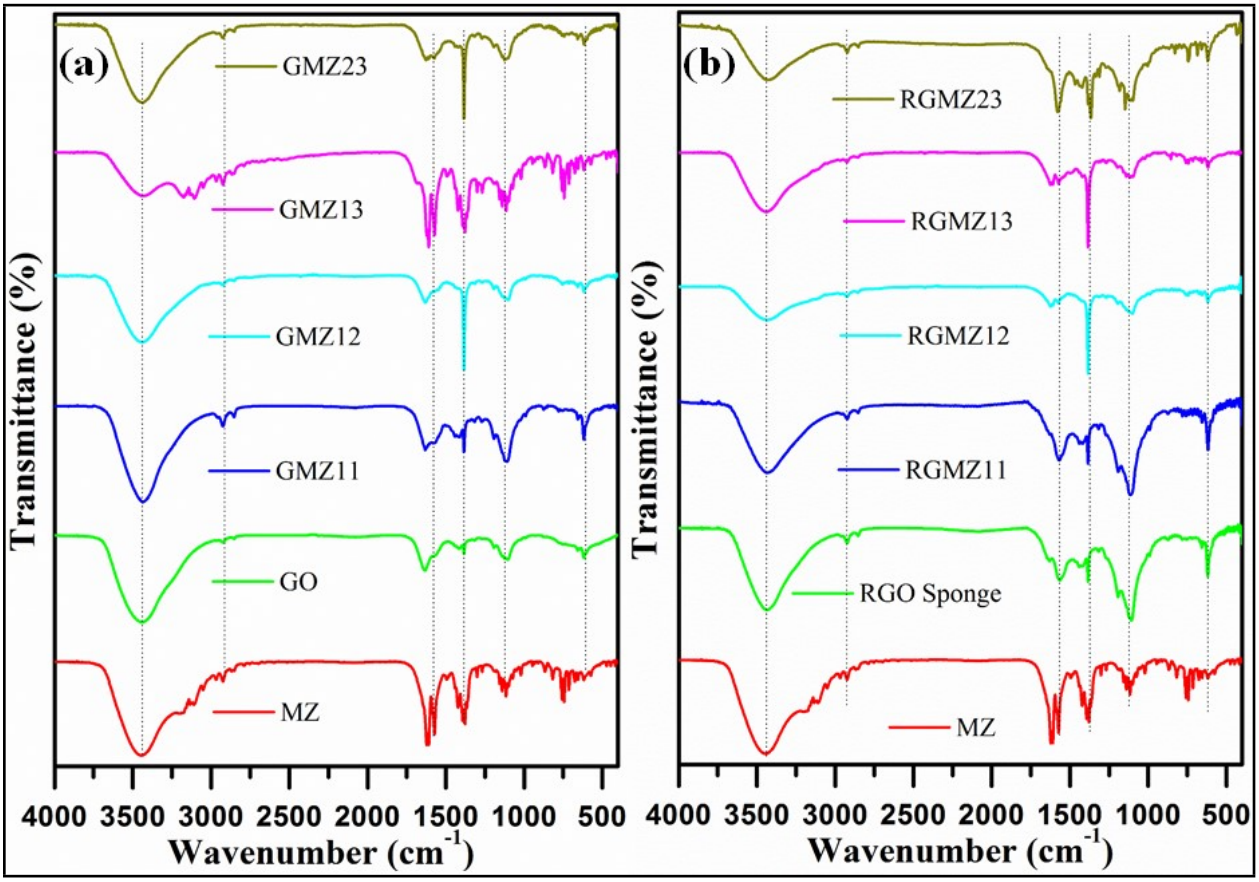

Figure S6. FTIR spectra: (a) MZ, GO, GMZ11, GMZ12, GMZ13, and GMZ23, (b) RGO sponge, RGMZ11, RGMZ12, RGMZ13, and RGMZ23.

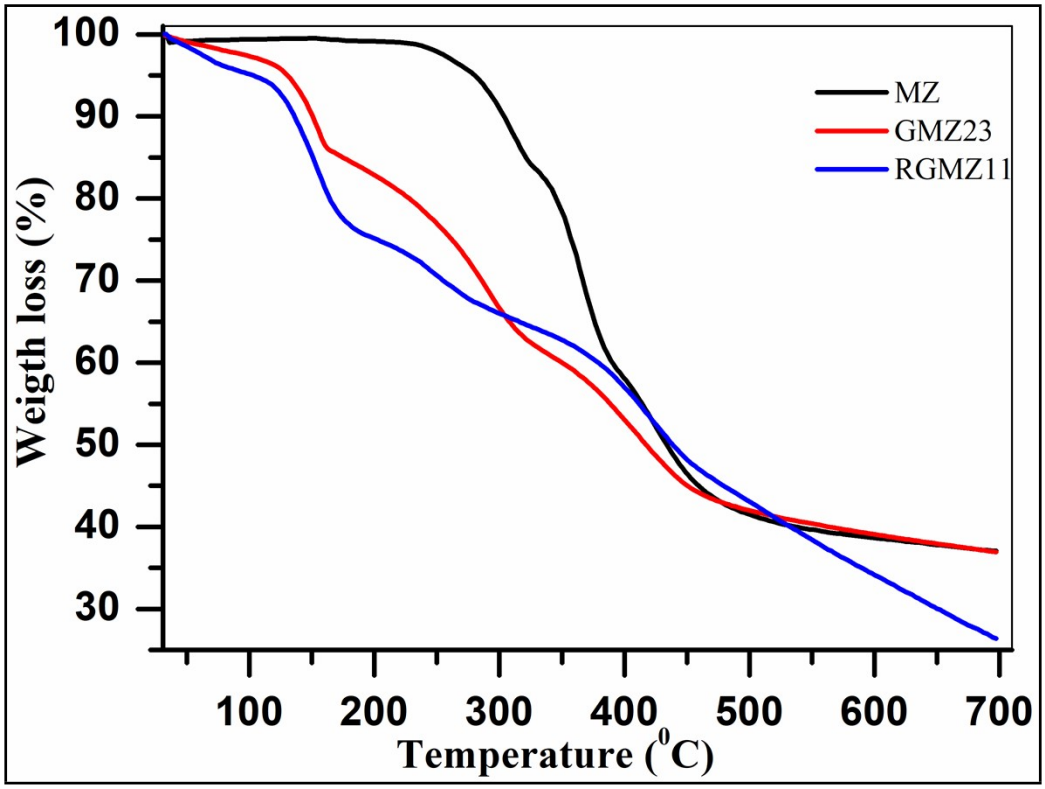

Figure S7. Thermogravimetric (TGA) pattern of MZ, GMZ23, and RGMZ11.

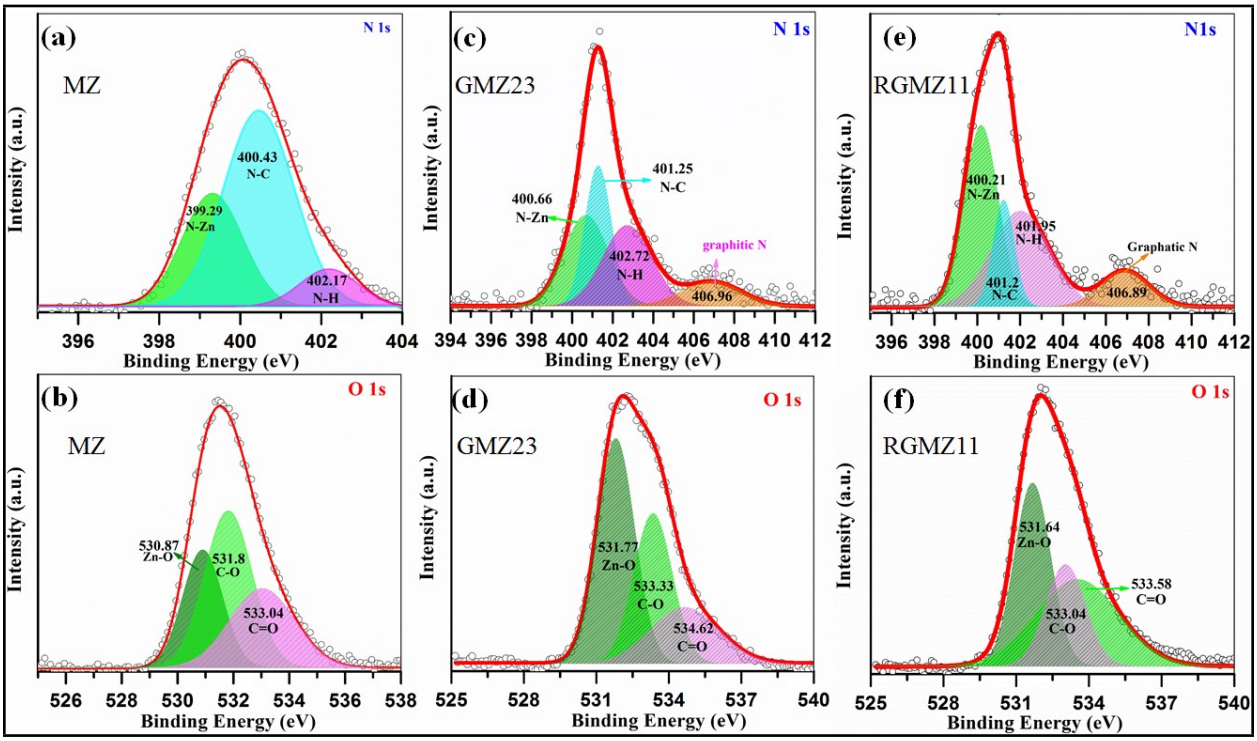

Figure S8. Deconvoluted XPS spectra of MZ for (a) N1s, and (b) O1s, for GMZ23, (c) N1s, (d) O1s, and for RGMZ11 (e) N1s, and (f) O1s.

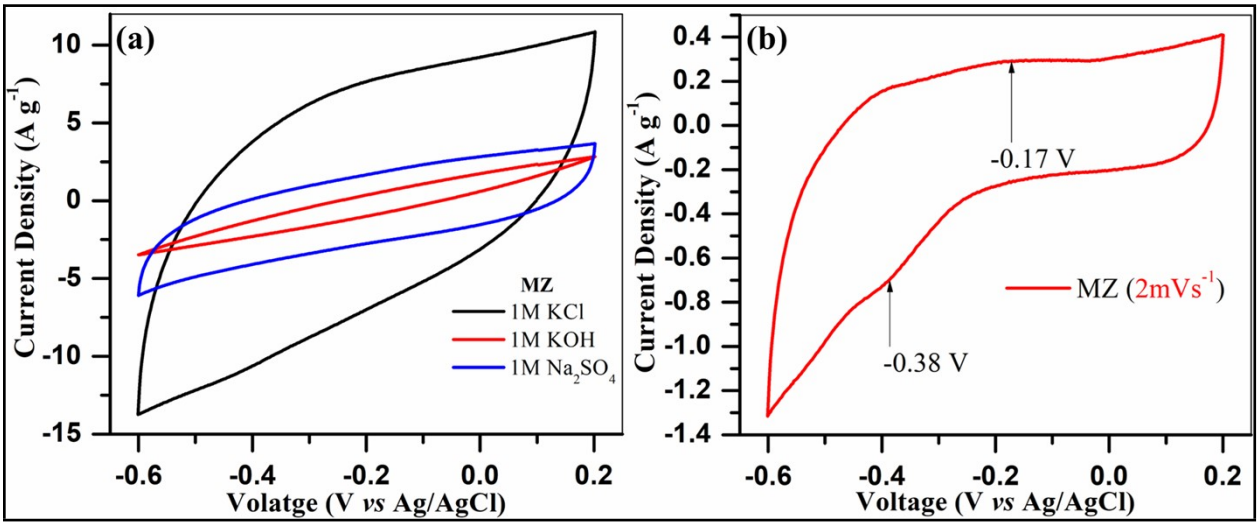

Figure S9. Electrolyte-based comparative study of MZ in 1M KCl, 1M KOH, 1M Na_2SO_4 at 100 mV s^{-1} within potential window range 0.2 to -0.6 V, redox behavior of MZ in aqueous 1M KCl at 2 mV s^{-1} within potential range of 0.2 to -0.6 V.

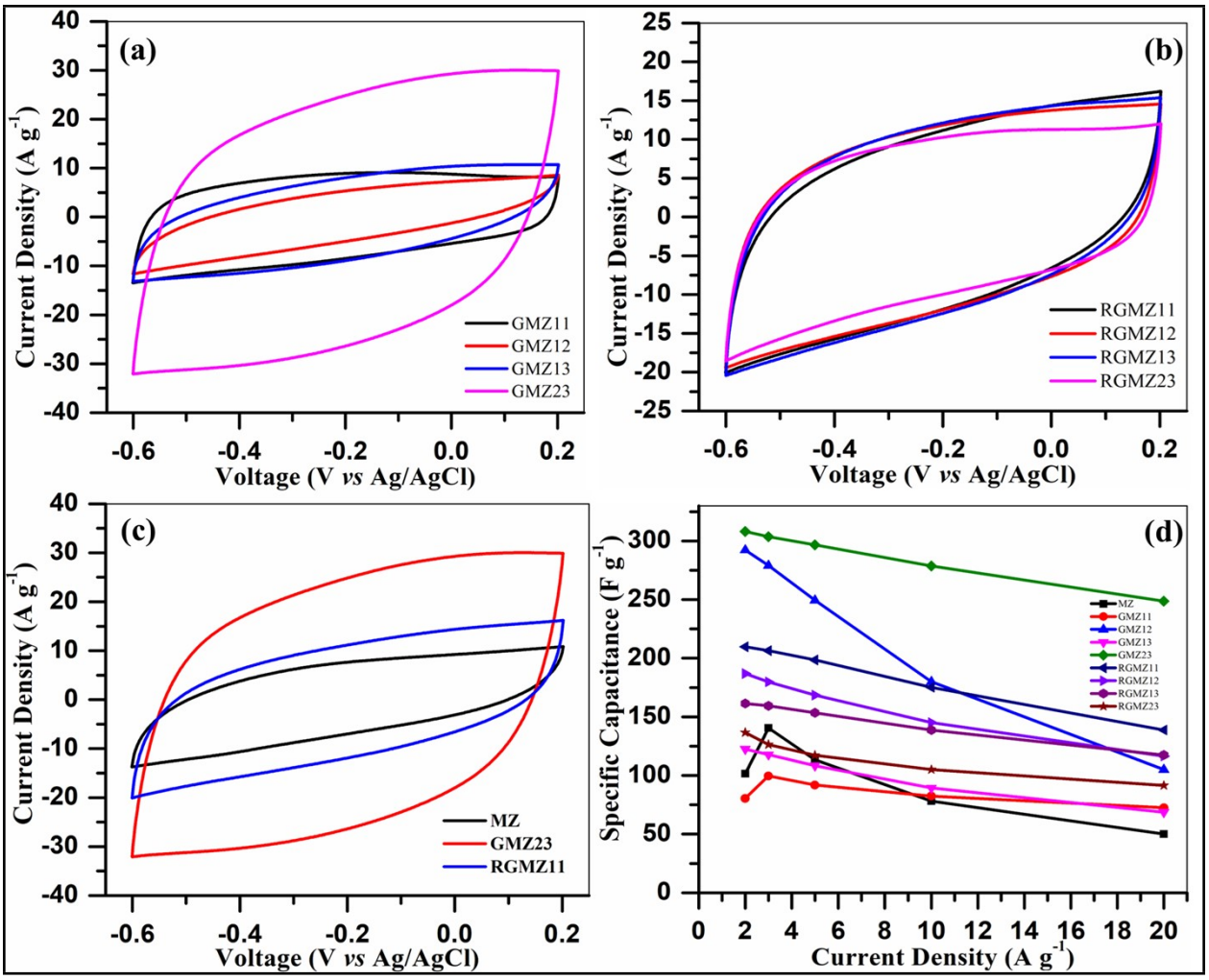

Figure S10. CV profile of (a) GMZ11, GMZ12, GMZ13, and GMZ23, (b) CV profile of RGMZ11, RGMZ12, RGMZ13, and RGMZ23 at 100 mV s^{-1}, (c) Comparative CV profile of best electrode material of GMZ and RGMZ series with MZ at 100 mV s^{-1} within a potential window of -0.6 to 0.2 V, (d) plotting of Current density (@ 2, 3, 5, 10, and 20 A g^{-1}) *vs* specific capacitance (F g^{-1}) of all prepared electrode materials.

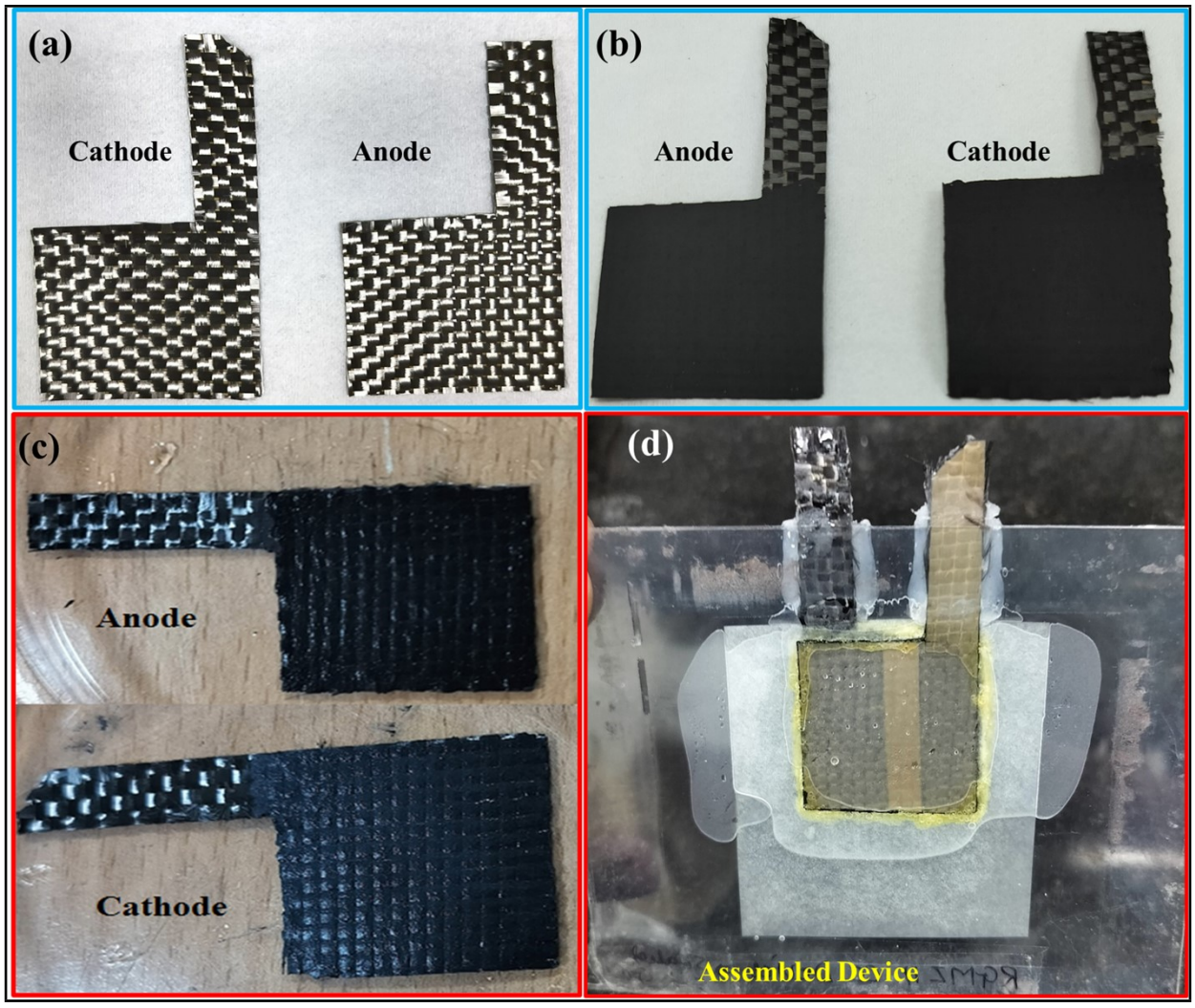

Figure S11. Images (a) bare carbon fiber of 3cm × 3cm, (b) coated with active materials, (c) soaked with electrolyte, (d) assembled ASC device.

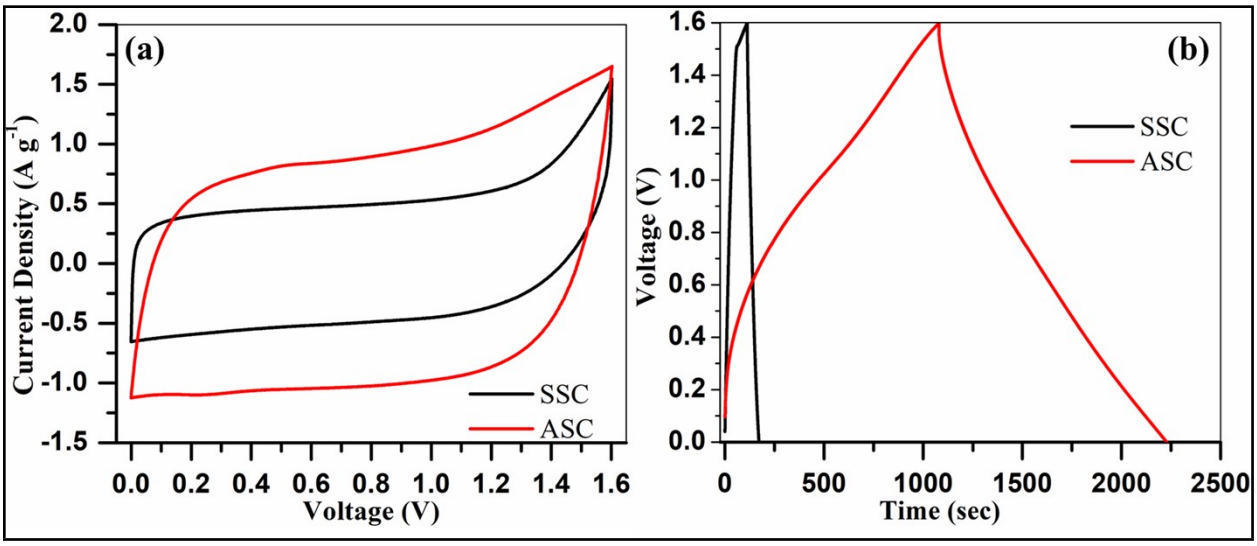

Figure S12. (a) CV and (b) GCD profile of SSC, and ASC device.

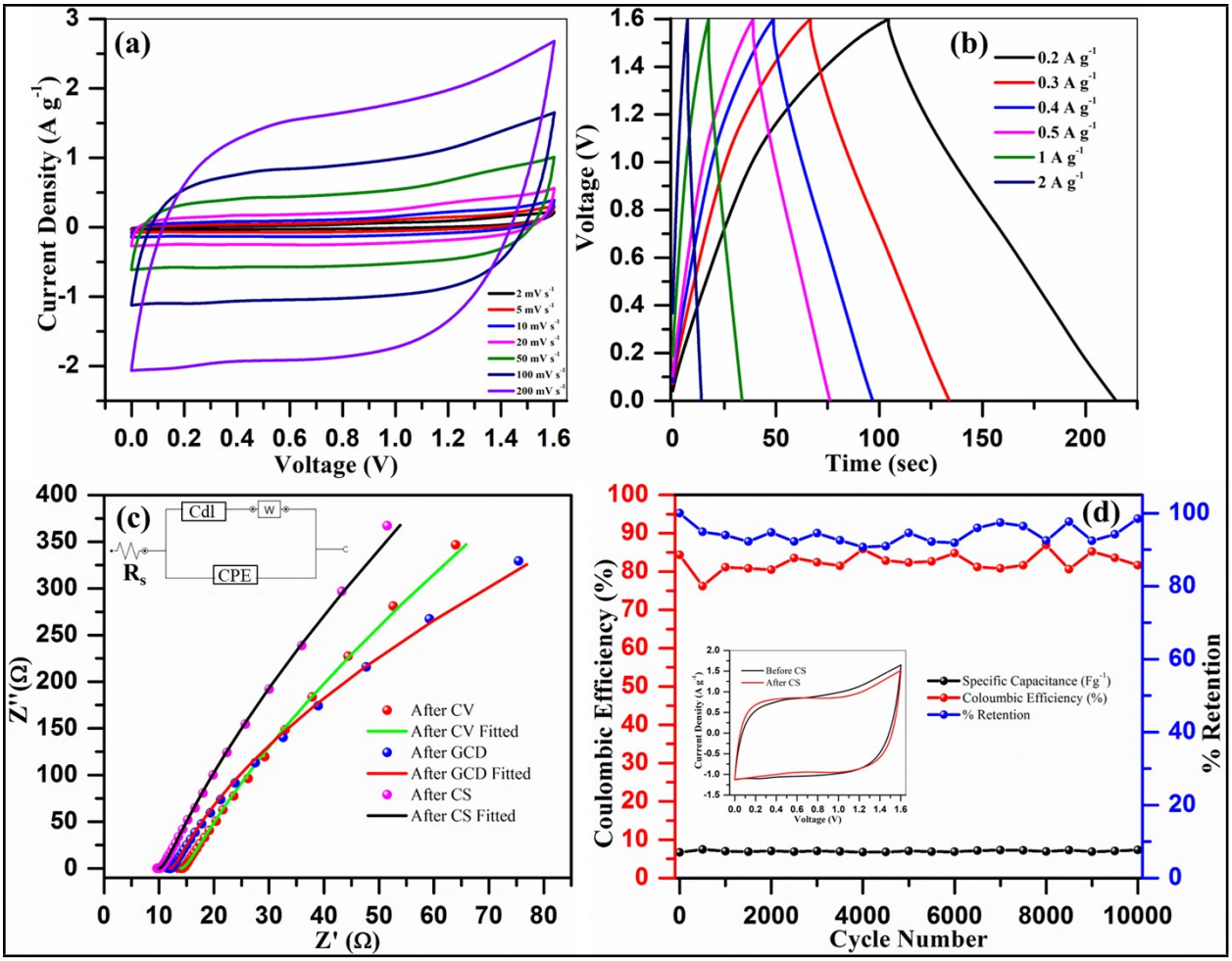

Figure S13. (a) CV profile of ASC device of MZ, (b) GCD at different current density, (c) EIS spectra of MZ after CV, after GCD and after CS (insert fitted circuit), (d) percentage retention, columbic efficiency (insert CV profile before cyclic stability and after cyclic stability).

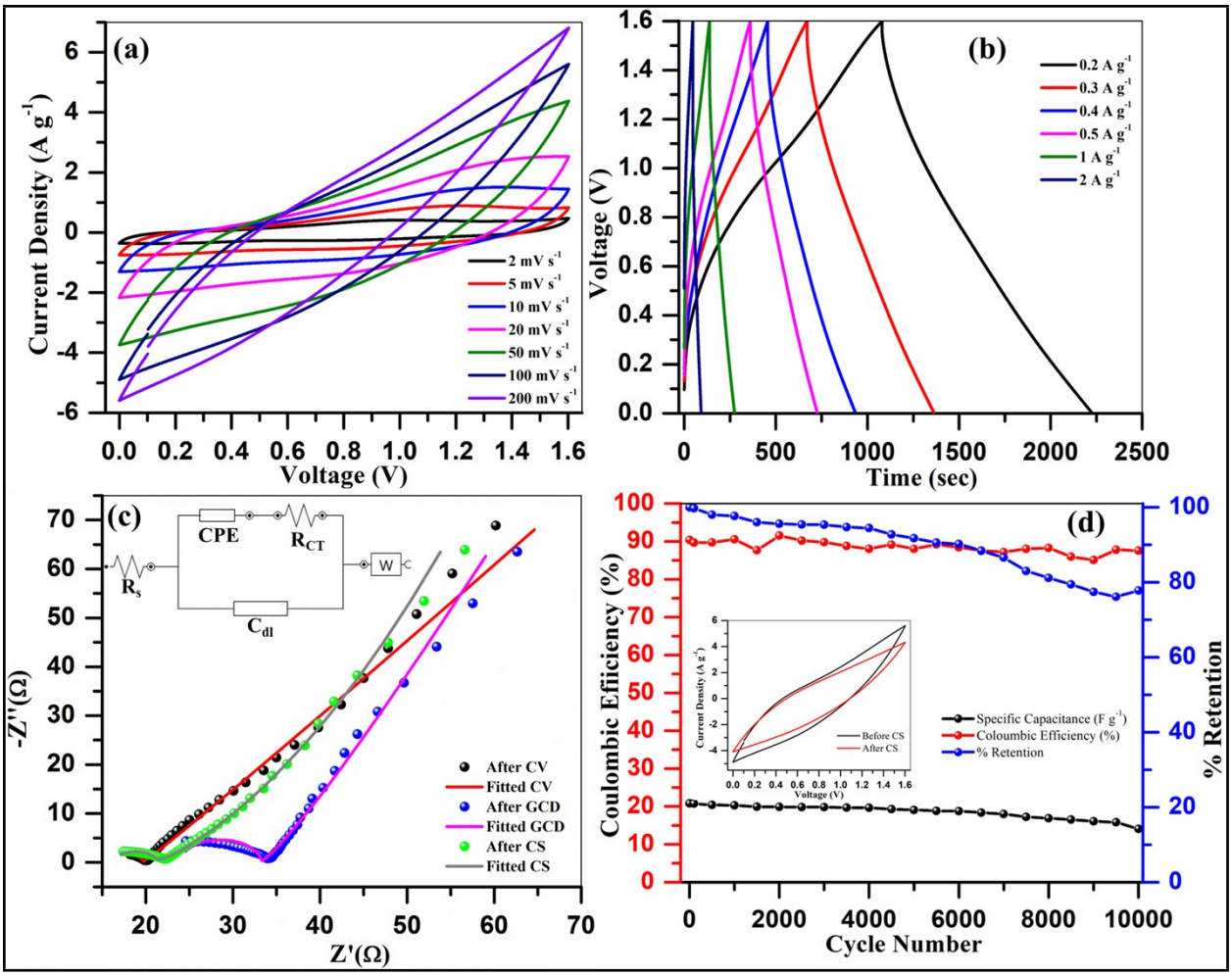

Figure S14. (a) CV profile of ASC device of GMZ23, (b) GCD at different current density, (c) EIS spectra of GMZ23 after CV, after GCD and after CS (insert fitted circuit), (d) percentage retention, columbic efficiency (insert CV profile before cyclic stability and after cyclic stability).

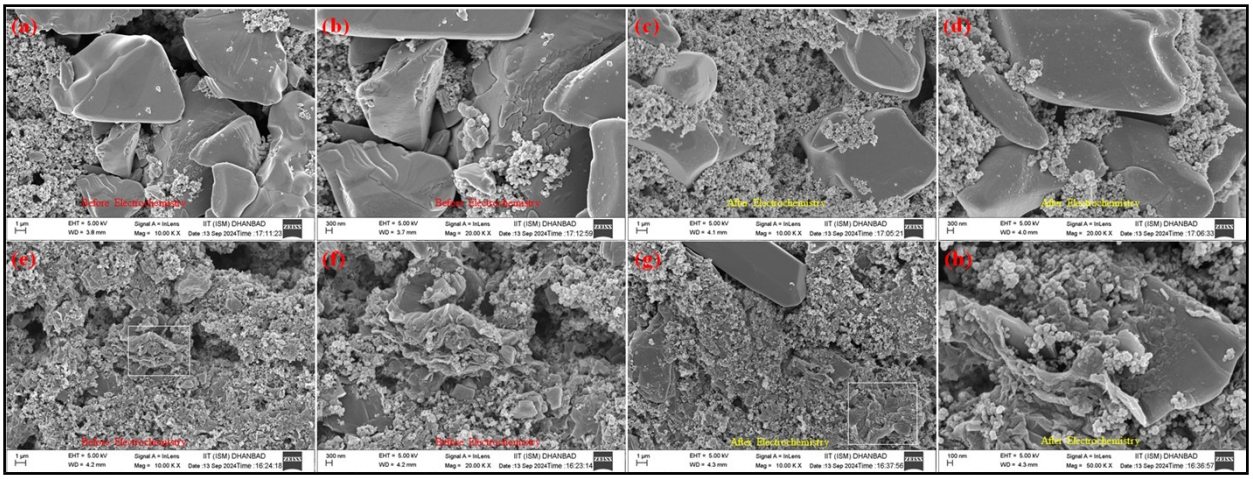

Figure S15. FESEM analysis of before and after ASC device at different magnification range, (a,b) before electrochemistry, (c,d) after electrochemistry of MZ; (e,f) before electrochemistry, (g-h) after electrochemistry of GMZ23.

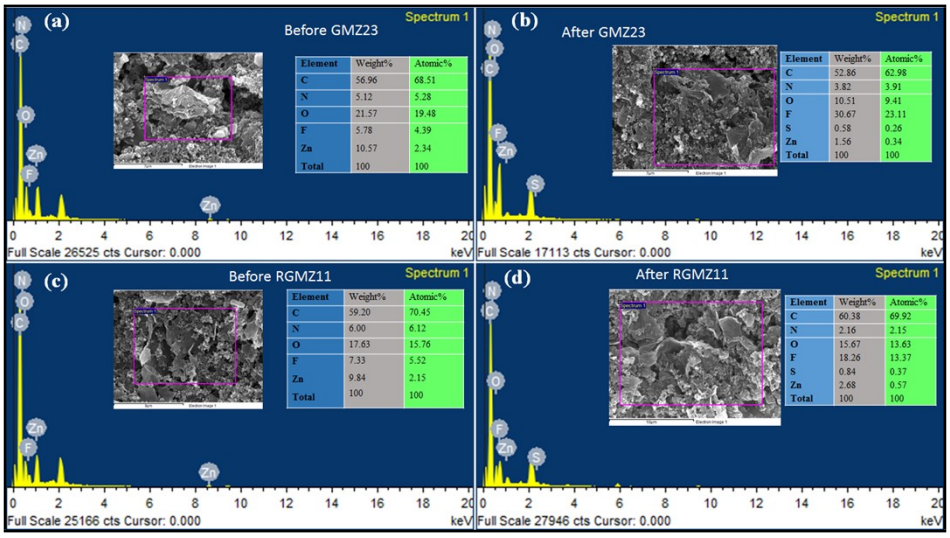

Figure S16. EDX analysis of ASC device (a) before and (b) after electrochemistry of GMZ23, (c) before and (d) after electrochemistry of RGMZ11.

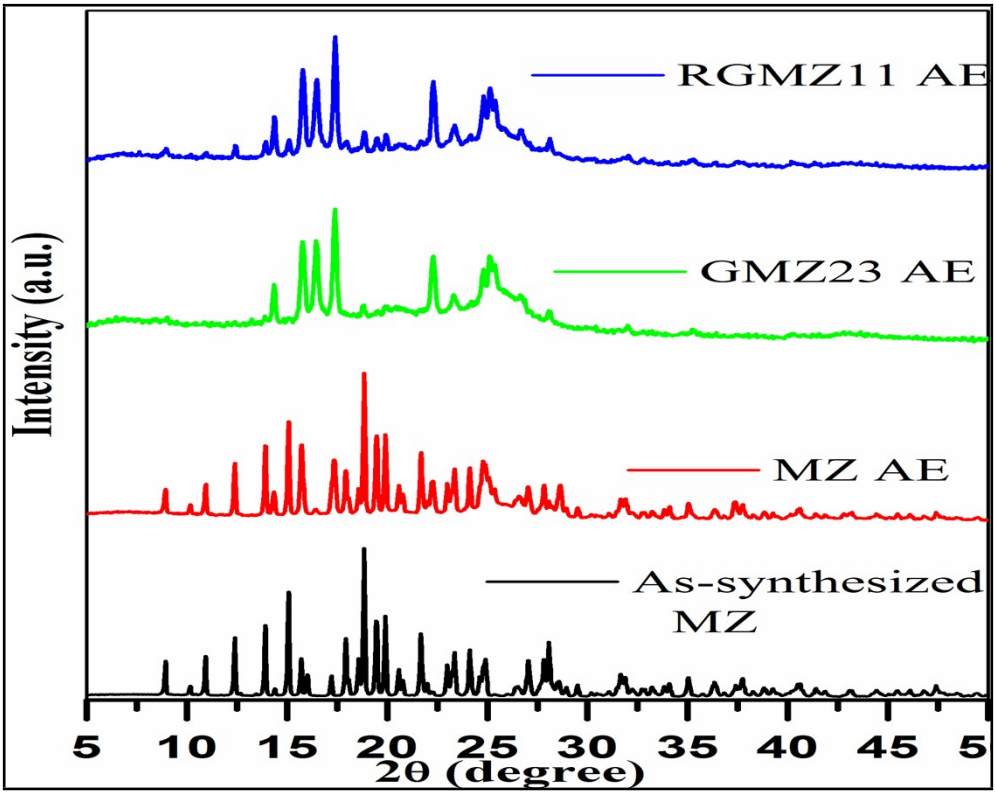

Figure S17. PXRD pattern after electrochemical performance of MZ, GMZ23, and RGMZ11 (AE: after electrochemistry).